Chemical Engineering Journal 96 (2003) 171–185

Chemical Engineering Journal

www.elsevier.com/locate/cej

Agglomeration in bio-fuel fired fluidized bed combustors

Weigang Lin*, Kim Dam-Johansen, Flemming Frandsen

Department of Chemical Engineering, Technical University of Denmark, Building 229, DK-2800 Lyngby, Denmark

Abstract

This paper presents results from systematic agglomeration experiments in a straw-fired laboratory-scale fluidized bed combustor and a theoretical study of the phenomena. Experiments were carried out at different operating conditions. Defluidization resulting from agglomeration occurred in all experiments. The agglomeration tendency is represented by the time before defluidization is detected. The results show that the temperature has a pronounced effect on the defluidization time, which can be significantly extended with decreasing temperature. Examination by various analytical techniques of the agglomerates sampled during combustion suggests that the high potassium content in straw causes the formation of agglomerates and eventually defluidization. In the combustion process, potassium-containing compounds are prone to remain in the bed and form low melting potassium-rich ash. The molten ashes coat the surfaces of the bed material, promoting agglomeration and defluidization in FBC.

Thermodynamic equilibrium calculations have been performed to identify the stable silica, potassium, chlorine and sulphur species. The results show that potassium silicates are the main form present in the bed, which agree qualitatively with the experimental results. Based on a competition between the strengthening adhesive force by the ash coating and sintering processes and the breaking force induced by bubbles in the bed, a simple model has been developed to describe the defluidization time as a function of temperature, fluidization velocity and particle size. The results are in good agreement with experimental results.

Keywords: Agglomeration; Biomass; Fluidized bed combustion; Defluidization

1. Introduction

Biomass is a potentially CO_2-neutral and renewable energy resource. As an alternative fuel it has attracted much attention worldwide in the recent years. Biomass was defined as organic non-fossil material of biological origin, a part of which constitutes an exploitable energy resource [1]. Biomass can be grouped into the following categories: wood residues, agricultural residues, dedicated energy crops and industrial and municipal waste of plant origin [2,3]. At present, biomass is converted into heat and electricity most often by combustion. In the last decade, many new biomass-based power plants have been built and process development is proceeding. Among these technologies, fluidized bed combustion (FBC) is an important process for utility-scale biomass power plants. This is due to the high combustion efficiency, low emission level and good fuel flexibility of the fluidization technology [4]. However, some biomass, especially the annual biomass has a high alkali content, which may form low melting point ash during combustion. The low melting ash constituents can induce formation of agglomerates in fluidized beds, in addition to deposition and corrosion. Accumulation of the agglomerates that are composed of sand and ash particles bound by fused, glassy materials, may lead to loss of fluidization (defluidization) and unscheduled shutdown of the plant [5–7]. In order to solve the operating problems from agglomeration in biomass fired FBC, a better understanding of the mechanisms is of essential importance.

1.1. Previous work on agglomeration and defluidization in a fluidized bed

1.1.1. Defluidization phenomena

In their pioneer work, Gluckman et al. [8] elucidated the features of defluidization phenomena. They demonstrated experimentally that addition of liquid into a gas fluidized bed leads to defluidization. Seville and Clift [9] explained the phenomenon by a changed ratio between particle gravity and inter-particle forces when a small amount of liquid was added to a fluidized bed. As the amount of liquid is increased, the fluidization behaviour of group B particles, classified by Geldart [10], can shift through group A to group C particles, which are difficult to fluidize. At high temperature, Gluckman et al. [8] showed that above a certain temperature, the

* Corresponding author. Tel.: +45-4525-2835; fax: +45-4588-2258.
E-mail address: wl@kt.dtu.dk (W. Lin).

1385-8947/$ – see front matter © 2003 Elsevier B.V. All rights reserved.
doi:10.1016/j.cej.2003.08.008

Nomenclature

b	radium of bonding neck
C	constant in Eq. (9)
C_1	ash accumulation constant
C_2	constant in Eq. (4)
C_3	constant in Eq. (5)
C_4	proportional constant in Eq. (8)
d	particle diameter
E_μ	activation energy for viscosity
f_K	weight fraction of potassium in the fuel
F_{ad}	adhesive force
F_{br}	breaking up force
n	number of particles in the bed
R	gas constant
t	time
t_{def}	defluidization time
T	temperature
T_s	initial sintering temperature
U	fluidization velocity
U_{mf}	minimum fluidization velocity without sintering
W	mass of bed material

Greek symbols

δ	thickness of the coating layer
μ	viscosity of melting ash
μ_0	pre-exponential factor of viscosity in Eq. (7)
ρ_{coat}	density of coatings
ρ_p	density of sand particles
σ	tensile stress of an agglomerate
ϕ_{fuel}	fuel feed rate to the bed

minimum fluidization velocity will not follow the theoretical value calculated by Ergun's equation [11], but increase sharply with temperature. They defined this onset temperature as 'initial sintering temperature', T_s. Thus, the minimum fluidization velocity as a function of temperature demonstrates two regimes delimited by the initial sintering temperature as shown in Fig. 1. It was found that T_s determined by the defluidization experiments coincides with that measured by a dilatometer [8,12–14]. Thus, the initial sintering temperature is an inherent property of particles and is governed by the chemical composition and characteristics of the particles. In a comprehensive review, Compo et al. [14] concluded that T_s can be significantly lower than the deformation temperature of ash by the conventional ASTM cone test. Skrifvars et al. [15–19] carried out systematic tests on T_s of ashes from various types of fuels in order to predict the sintering tendency under FBC and gasification conditions. They found that the initial sintering temperature is a much better predictor than the ASTM method for the agglomeration tendency in FBC.

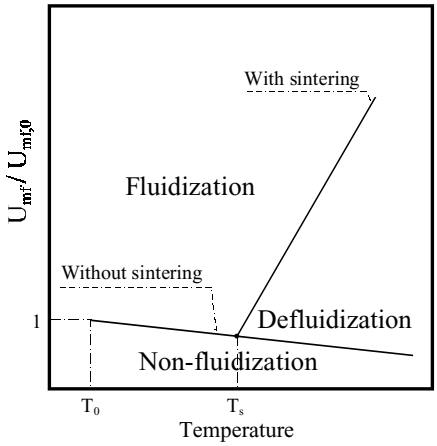

Fig. 1. Fluidization diagram at high temperature with and without sintering effects (adapted from [12,14]).

1.1.2. Formation and identification of coating layer

Many researchers have been working on the identification of the adhesive material in FBC of different types of low-rank coals. Dawson and Brown [20] reported that sticky aluminosilicate material acted as a glue to form agglomerates when burning high sulphur coal in a laboratory-scale FBC. In combustion of low-rank coals with a high content of sulphur and sodium, Manzoori et al. [21,22] showed the presence of a molten phase coating, which is rich in sodium, calcium and sulphur. Anthony et al. [6,23] found severe agglomeration in the loop-seal of a CFB boiler when firing petroleum coke. They reported that not only vanadium but also the sulphated limestone contribute to the agglomeration process. These results provide information of the compounds responsible for agglomerate formation from different fuels.

For a better understanding of the agglomeration phenomena, another question needs to be addressed: How are these compounds transferred to the surfaces of the bed material? Mann et al. [24] suggested that deposition and condensation of volatile ash species on the surfaces of bed material is the major way of transfer. Manzoori et al. [21] showed a continuous transfer of coal ash from the char to the surfaces of bed material, indicating that the ash is transferred by the collisions between particles in the bed.

1.1.3. Biomass

The investigations summarized above are for combustion or gasification of coal. The ash characteristics of biomass are different from those of coals. Though the compositions vary with plant types and the growth conditions, biomass ashes are normally dominated by silicon, calcium and potassium and contain little aluminium [25]. Potassium is dispersed in biomass in ionic and organometallic forms, while silicon occurs primarily as hydrated silica grains. During combustion, potassium is likely to be volatilized with organic species. It may be released as KCl if chlorine is present in the fuel. Without chlorine, hydroxides, oxides, sulphates or carbonates may be formed [5]. Olanders and

Steenari [25] found that alkali and alkaline earth metal ions associate primarily with sulphate, carbonate and chloride ions during ash formation. Skrifvars et al. [18] applied various methods to characterize different types of biomass ashes. They reported that the elemental compositions of the ashes did not change significantly with ashing temperature. These findings indicates that most potassium compounds may not be released to the gas phase, but tend to remain in the ash matrix by recapture of the vapours by some mineral components in the ash under FBC conditions.

Studies have been reported on agglomeration and defluidization phenomena in FBC or gasification of biomass. Ergüdenler and Ghaly [26] carried out gasification experiments of wheat straw in a fluidized bed with silica sand as bed material, showing that agglomerates were formed when temperature approached 800 °C and severe defluidization occurred as soon as the temperature exceeded 800–820 °C. They concluded that the high fraction of potassium in straw ash was the major contributor to this phenomenon. Salour et al. [27] reported that defluidization occurred in a pilot scale FBC during combustion of straw. They showed that blending straw with wood reduced the tendency of agglomeration but did not eliminate the problem. Grubor et al. [28] reported agglomeration and defluidization problems in a 150 kW continuously straw-fired FBC, which led to 2–3 times shutdown in a month even though the temperature was below 700 °C. They suggested using alternative bed materials, e.g. ferric oxide, to avoid formation of low melting temperature eutectic compounds of alkali-silicates. However, the results mentioned appear rather preliminary and mechanisms were not discussed in detail. Nordin et al. [29] and Skrifvars et al. [19] tested the agglomeration behaviours of different biomass ashes in a pilot scale fluidized bed combustor more systematically, with programmed temperature change without combustion. They examined the defluidization temperature, at which the sand bed containing biomass ash was defluidized, and found that this temperature is close to the initial sintering temperature of the ash determined by the compression strength method. Olofsson et al. [30] reported the agglomeration problems in pressurized FBC of biomass.

1.1.4. Modelling

Several models have been developed to predict the minimum fluidization velocity at high temperatures, i.e. the fluidization diagram at high temperature as shown in Fig. 1. Basu [12] and Liss et al. [31] rewrote Ergun's equation by including an adhesive force in the force balance. They correlated the adhesive force with the excess temperature ($T - T_s$) and derived the expressions of minimum fluidization velocity as a function of temperature. Tardos et al. [32,33] compared the breaking forces acting on agglomerates and the agglomerate strength to predict the limiting velocity to defluidize. Considering kinetic energy dissipation upon collision of two particles to determine whether or not two particles will stick to each other, Moseley and O'Brien [34] developed a model for calculation of defluidization velocity as a function of temperature. They introduced a 'surface adhesiveness coefficient' to account for the temperature effect, in which the correlation of Liss et al. [31] was applied. In a similar approach, Ennis et al. [35] mapped the defluidization limit by using a critical viscous Stokes number for defluidization. Seville et al. [36] proposed a model by comparing the residence time of agglomerates in the quiescent zones and the sintering time to predict the defluidization velocity.

In these models, the time dependence of agglomeration phenomena was not considered [27]. Yang et al. [37] proposed a model to predict the extent of agglomeration in a fluidized bed with a central jet. The model included mass and momentum balances to describe the fluid dynamics, and collision number and adhesion probability to describe the agglomeration rate. But, the defluidization phenomenon was excluded in their model.

1.1.5. Objectives of the present work

Although substantial work has been performed on agglomeration and defluidization phenomena in FBC and gasification, the understanding of the mechanisms is yet far from complete. Several mechanisms need to be understood of agglomeration and defluidization in FBC: Which compounds are responsible for the particles in the bed becoming adhesive? How are these compounds transferred to the particle surface? How do the adhesive particles affect the fluidization behaviour and formation of agglomerates? And what are the important parameters affecting defluidization? The main objective of this work is to study the ash behaviour of one of the most troublesome biomass, wheat straw, on agglomeration in FBC in order to obtain more knowledge on the mechanisms of the agglomeration. Different analytical techniques are applied and thermodynamic equilibrium calculations are performed. Based on the experimental findings and calculating results, a simple model has been developed to describe the agglomeration and defluidization processes in a straw-fired fluidized bed combustor.

2. Experimental

2.1. Apparatus

Experiments were carried out in a laboratory-scale fluidized bed combustor. The experimental apparatus, schematically shown in Fig. 2, consists of three parts: reactor section, dosing section and analysis and data acquisition section.

The reactor is made of high temperature resistant steel tube with an inner diameter of 68 mm. The total height of the reactor is 1.2 m. A perforated steel plate distributor is located at a height of 0.6 m. Below this position is the preheat zone and above is the combustion zone. The reactor is electrically heated by three independently controlled heating elements. The pressure drop over the bed was monitored by two pressure transducers at the top and at the bottom of the

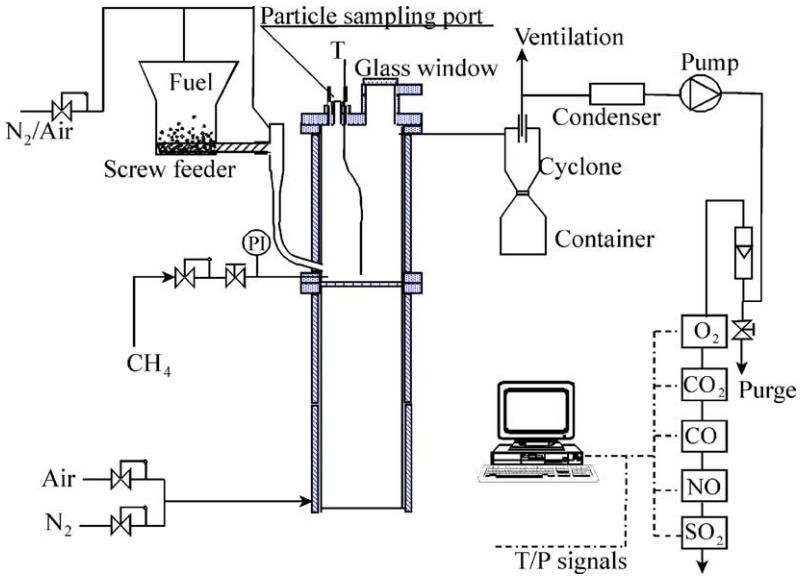

Fig. 2. Schematic view of the experimental apparatus.

bed. The temperature profile in the bed was continuously measured by thermocouples. The combustion and fluidization behaviours can be visually observed through a window in the reactor top. Particles can be sampled from the top port during experiments.

Fuel is stored in a container and can be continuously fed to the bottom of the combustor by a screw feeder with various feeding rates. Compressed air and N_2 from a gas cylinder, controlled by precision mass flow controllers (MFCs), are fed partly to the bottom of the reactor and partly to the fuel feeding system to prevent the pipeline from blockage. Natural gas can be fired in the bottom of the bed before introducing the solid fuel in order to smooth the bed temperature transition at starting fuel feed. The elutriated fines in the flue gas are separated from the gas by a cyclone and collected in a container. Most of the flue gas is lead to a vent. A small amount of the flue gas is induced by a pump to a series of gas analysers to monitor the concentrations of O_2, CO_2, CO, NO and SO_2. Water is removed by a condenser before the gas enters the analysers.

2.2. Fuels and bed materials

The fuel used was Danish wheat straw. The straw was pelletized to a size range 1–10 mm in order to avoid feeding problems. The proximate and ultimate analyses of the straw pellets are shown in Table 1. The standard analysis of the ash is shown in Table 2. For a comparison, a small batch of the straw ash was prepared at 880 °C under oxidizing condition. The results are also given in Table 2. It is shown that some inorganic constituents, especially the potassium constituent have little difference between the ashes obtained by the two methods.

Quartz sand (98.9% SiO_2, melting temperature 1450 °C) with various size ranges is used as bed material in the experiments. In all experiments the same amount of sand particles were used with a bed height of approximately 110 mm during fluidization.

2.3. Experimental

Combustion experiments were carried out in the apparatus to study the influence of different operating parameters, such as temperature, combustion stoichiometry, gas velocity and particle size of the bed material, on the defluidization time. During the experiments only one parameter was varied compared to the reference case, the remaining parameters were kept constant. The operating conditions are summarized in Table 3.

The fluidized bed reactor was first heated to a preset temperature and then an amount of methane, with a heating value equivalent to that of the planned straw feed, was introduced to the bottom of bed. When the temperature reached a stable level, the methane was switched off and straw was fed into the bottom of the bed. In this way, the bed temperature was kept constant after straw was introduced. During the experiments the pressure drop over the bed, temperature profile inside the bed and the concentrations of O_2,

Table 1
Characteristics of the wheat straw

Proximate analysis (wt.%, as delivered)[a]		Ultimate analysis (wt.% DAF)	
Volatile	69.5	C	48.84
Fixed carbon[b]	16.7	H	7.08
Ash	7.3	O	41.56
Moisture	6.5	N	1.28
		S	0.23
		K	1.01

[a] High heating value: 17.24 MJ/kg and low heating value: 15.78 MJ/kg.
[b] Not measured, calculated by difference.

Table 2
Analysis of the straw ash (wt.%)

	SiO_2	Al_2O_3	Fe_2O_3	CaO	MgO	Na_2O	K_2O	SO_3	TiO_2	P_2O_5
Standard ash	39.00	0.95	0.95	9.9	2.2	0.44	29	3.3	0.4	4.7
Ash (880 °C)	50.17	0.47	0.47	12.15	3.09	0.87	26.37	0.95	0.07	5.1

Table 3
Experimental conditions

Parameter	Reference	Range
Temperature (°C)	830	725–930
Stoichiometric factor, λ (–)	1.2	1.0–2.6
Gas flow rate, Φ_{air} (N l/min)	14	14–28
Particle size of bed material, d (mm)	0.275	0.275–0.46

CO_2, CO, NO and SO_2 were continuously monitored and logged to a computer. In the course of the experiments, particle samples were taken from the bed regularly for further analysis. The defluidization is marked by a sharp decrease in the pressure drop over the bed. As soon as defluidization occurred, straw feed was stopped. The time between the start of straw feeding to defluidization of the bed is defined as the 'defluidization time'. A few batch experiments were performed to identify the agglomerates initiated on the burning char particles. About 0.5 g of straw pellets in a basket with a hole size of 4 mm, large enough for sand particles to move in and out freely, was inserted into the bed at various temperatures and kept for different time periods. The particle samples inside the basket were taken out of the reactor, and quickly put into a container with liquid N_2 in it for a fast quench. The burnout behaviour of the straw pellets was examined by tracing the O_2, CO_2, CO and NO concentrations.

The particles sampled during combustion were analysed by various analytical techniques. Simultaneous thermal analysis (STA) was used to examine the melting behaviour of the agglomerates and straw ash. The procedure was described in detail elsewhere [38]. X-ray diffraction (XRD) was applied to identify the different mineral compounds present in agglomerates. Morphology of agglomerates and the elemental distribution on their surfaces were obtained by SEM/EDX analysis. Various series of particles sampled from the bed at different temperatures were chemically analysed to study the gradual accumulation of the potassium compounds in the bed. Each sample was first leached in dilute sulphuric acid. The solution was then filtered, and its ionic content was determined by ion chromatography.

3. Results

3.1. Influence of parameters on the defluidization time

Defluidization occurred in all performed combustion experiments. The main parameter to be studied in the experiments is the defluidization time, t_{def}. The defluidization is indicated by a sudden decrease in the pressure drop over the bed. The temperature profile inside the bed is another indicator of defluidization. When the bed is in normal fluidization state, the bed temperature is very uniform. Just before defluidization occurs, the difference between the temperature at the bottom of the bed and that 2 cm above becomes larger due to poor mixing. It is noticed that the pressure drop declined slowly before defluidization occurred at relatively low combustion temperatures, suggesting a segregation of large agglomerates to the bottom of the bed.

In order to test the reproducibility, several experiments at different temperatures, flow rates and particle sizes were repeated. The results of repeated experiments are summarized in Table 4. It shows a good reproducibility with respect to the defluidization time.

3.1.1. The influence of bed temperature

During combustion experiments, the variation of the temperature was small (within 5 °C). The average temperature 2 cm above the distributor is used as bed temperature. The defluidization time as a function of bed temperature is plotted in Fig. 3. The results show that the influence of temperature on the defluidization time is significant. As the temperature decreases, the defluidization time increases. As temperature increases, the fraction of ash melt increases and the viscosity of the melt decreases. The combination of these two factors results in an increase of the stickiness of the sand particle coated by the ash. This accelerates the defluidization process.

3.1.2. The influence of gas velocity

In all experiments, the influence of gas velocity was examined by changing the gas flow rate. The combustion stoichiometry was kept the same by mixing air with N_2. The

Table 4
Summary of the reproducibility of the experiments

	$d = 0.275$ mm, $\Phi_{air} = 14$ N l/min				$d = 0.388$ mm, $\Phi_{air} = 17.5$ N l/min				$d = 0.46$ mm, $\Phi_{air} = 24.5$ N l/min	
T (°C)	796	797	822	823	843	845	866	869	819	820
t_{def} (min)	42.1	45.2	26	26.4	19.3	19.2	18.3	17.7	26	26.5

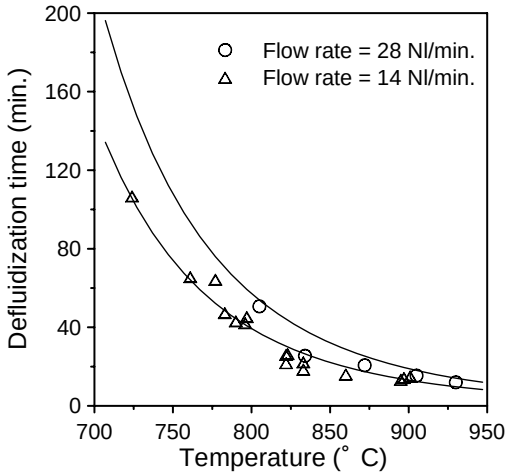

Fig. 3. Influence of temperature on the defluidization time at two air feeding rates.

experimental results demonstrate that the defluidization time will be extended as the gas flow rate increases. This trend is shown in Fig. 3. When the gas flow was doubled the defluidization time was about 30% longer. The higher gas velocity in the bed will lead to a better mixing of the particles and increase the force acting on agglomerates, induced by bubbles. The better mixing and higher breaking rate of formed agglomerates will prolong the defluidization time.

3.1.3. The influence of the particle size

The effect of the sand particle size on the defluidization time is shown in Fig. 4. At the same gas velocity and combustion temperature, an increase of particle size leads to a shorter defluidization time. Larger particles have a lower specific outer surface area. This will result in a thicker ash coating layer. In addition, the minimum fluidization velocity is higher for larger particles. Thus, the ratio of U/U_{mf} is lower, the mixing in the bed will not be as good as for the smaller particles. These two factors will both accelerate

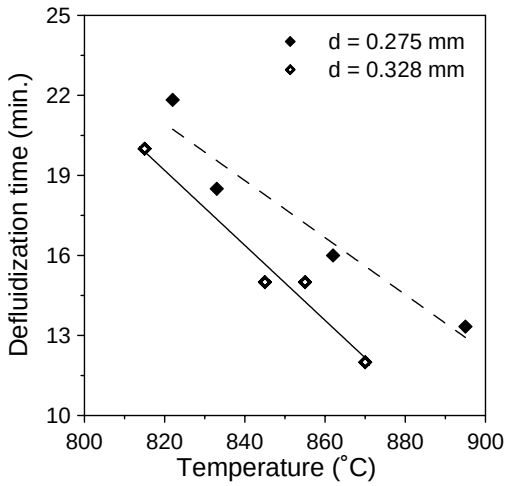

Fig. 4. Influence of sand particle size on the defluidization time.

the defluidization. The influence of gas velocity and particle size of bed material in this work is in agreement with that reported by Atakül and Ekinci [39] in studying agglomeration in FBC of Turkish lignites.

One experiment with smashed straw pellets (<1 mm) has been carried out to examine the influence of the size of straw pellets. It appears that the fuel size has no effect on the defluidization time.

3.1.4. The influence of combustion stoichiometry

At 830 °C the defluidization time seems to increase slightly with increasing stoichiometric factor in the range from 1 to 2.5. It has been shown that the effect of combustion stoichiometry on defluidization time is minor [40]. Two factors may influence the agglomeration process with respect to the combustion stoichiometry. On the one hand, it is expected that the defluidization time will be shortened at lower stoichiometry because of the usual lower melting temperature of ash under reducing condition. On the other hand, the temperature of a burning particle may be lower at low stoichiometry than at high one, which may extend the defluidization time. The combination of the two factors may result in a minor effect of combustion stoichiometry on the agglomeration tendency. From experimental investigations, Skrifvars et al. [16,18] reported that reducing conditions have little influence on the sintering temperature of coal ashes and biomass ashes from laboratory sintering experiments. This is consistent with our results.

3.2. Melting behaviour of agglomerates and straw ash

The melting behaviour of two batches of agglomerates, sampled after defluidization has been examined by STA in a N_2 atmosphere. Unfortunately, only the transition temperature from α-quartz to β-quartz around 570 °C was observed from the differential scanning calorimetry (DSC) curve. No melting has been identified from these samples, probably due to the fact that too little ash was present in the samples.

A straw ash sample, prepared at a temperature of 880 °C in oxidizing condition, was tested by STA at the same condition as for the agglomerate test. The DSC and mass change curves over a temperature range up to 1200 °C are shown in Fig. 5. The weight percentage of melt, estimated by integrating the area under the DSC curve [38], as a function of temperature is also shown in Fig. 5.

The results show that the straw ash starts to melt already at 750 °C. Only a very small amount of ash (about 2%) was evaporated, starting at about 900 °C indicated by a decrease in the mass loss curve. This result may well be representative to the straw ash behaviour in the combustor.

3.3. XRD analysis

A batch of particles, sampled after long time straw-firing with several defluidization and forced refluidization processes, was analysed by XRD. The spectrum of an X-ray

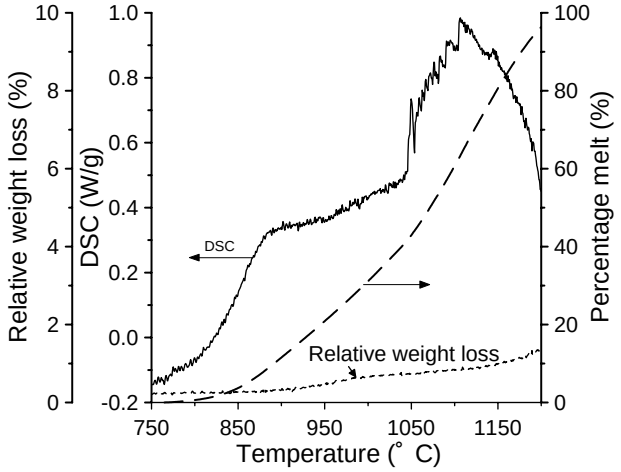

Fig. 5. Melting behaviour of the straw ash by STA.

exposure of a single sand particle showed only the lines of quartz. The results from a group of sand particles showed the spectrum of potassium feldspar ($KAlSi_3O_8$). The potassium feldspar probably exists as small inclusions in this group of sand particles rather than as a part of ash. The results indicate that the ash coating on the sand surface may be too thin to be detected by this method. The conclusion is consistent with the results from STA of agglomerate samples. Another possible reason is that the coating is not crystalline, but has upon cooling formed amorphous phases.

3.4. Accumulation of potassium in the bed material

The accumulation of potassium in the bed at different temperatures is shown in Fig. 6. The straight line in the figure represents the theoretical potassium content in the bed calculated from the straw feed rate and K-content in the straw pellet shown in Table 1, assuming that all potassium accumulates in the bed. Though the results show some scattering, probably caused by heterogeneity of the samples, the trend is clear that the potassium content in the bed increases with time and the increase is close to linear. As time increases, the K-content in the bed tends to be lower than the theoretical value. This may be due to the elutriation of K-containing fine ash particles, whose amount will increase with time. From Fig. 6, it is shown that the influence of combustion temperature on the potassium build-up is minor at least up to 900 °C. This indicates that potassium compounds in straw tend to remain in the bed and little is evaporated during combustion in the temperature range between 810 and 900 °C. The results are consistent with the results from STA, which shows that only a little evaporation occurred of the ash sample up to 1100 °C. In order to confirm this trend, an experiment was carried out at 870 °C. The bed defluidized 12 min after start of fuel feeding. Then the straw feed was stopped and the bed was forced to refluidize by stirring with a metal rod. The bed temperature was kept the same by firing methane. The bed was defluidized and refluidized three times. At each time of defluidization, particles were sampled. The samples were chemically analysed and the results are presented in Fig. 7. It is shown that the potassium content in the bed material did not decrease, indicating that potassium is not released to the gas phase from straw ash in the bed, which is in agreement with the STA results of the straw ash. The increase of the potassium content in the last point may again be caused by the heterogeneity of the sample. Duplication of the analysis shown in Fig. 7 suggests that the reproducibility of this method is good.

3.5. Morphology and composition of agglomerates

All agglomerates collected could be easily broken by a finger touch. Different sizes of agglomerates exist, some

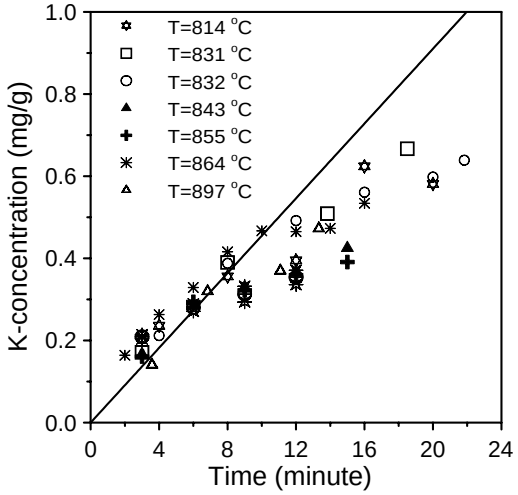

Fig. 6. Accumulation of potassium in the bed during combustion at different temperatures.

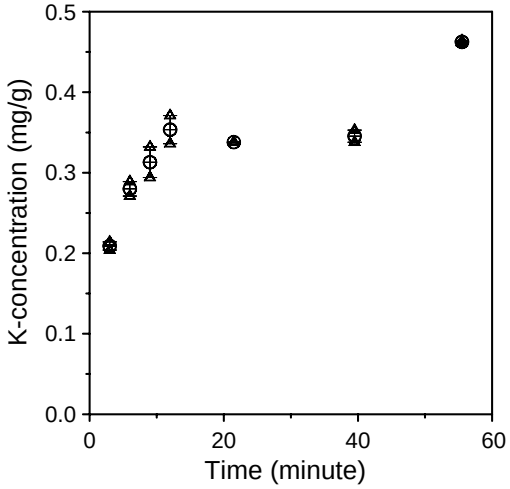

Fig. 7. Potassium content in the bed during combustion of straw and after stopping feeding straw with duplicated analyses.

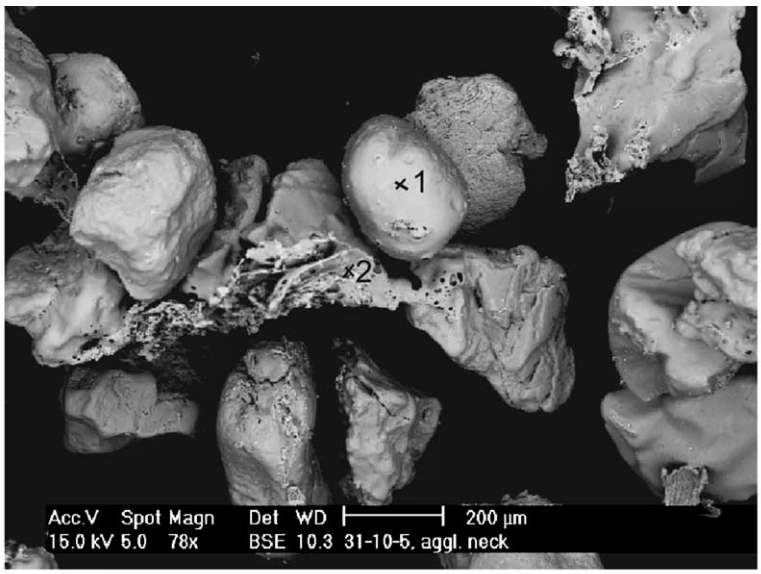

	SiO_2	Al_2O_3	Fe_2O_3	CaO	MgO	Na_2O	K_2O	P_2O_5
Point 1 (wt.%)	78.01	0.26	0.31	0.27	0.11	0.86	20.04	0.14
Point 2 (wt.%)	62.81	0.38	0.00	5.70	3.77	0.80	22.05	4.49

Fig. 8. SEM image of particles and EDX analyses at two points on the surface (sampled after defluidization, $T = 815\,^{\circ}C$).

being of the same size as the fuel pellets (∼5 mm) and others consisting of only a few sand grains glued together (∼1 mm).

Some of the agglomerates, sampled in the course of the experiments, were examined by SEM/EDX analysis. A typical SEM image of a sample is shown in Fig. 8. The sand particles are sticked together by necks. Ash flakes link a few particles as well. Some of the grain surfaces are covered with small pieces of the ash, but most of the sand surfaces look smooth. EDX analysis on an ash flake shows that the composition is similar to that of ash (point 2). At a smooth sand surface (point 1), the major elements are silicon and potassium with 20 wt.% present as K_2O. This indicates that not only ash

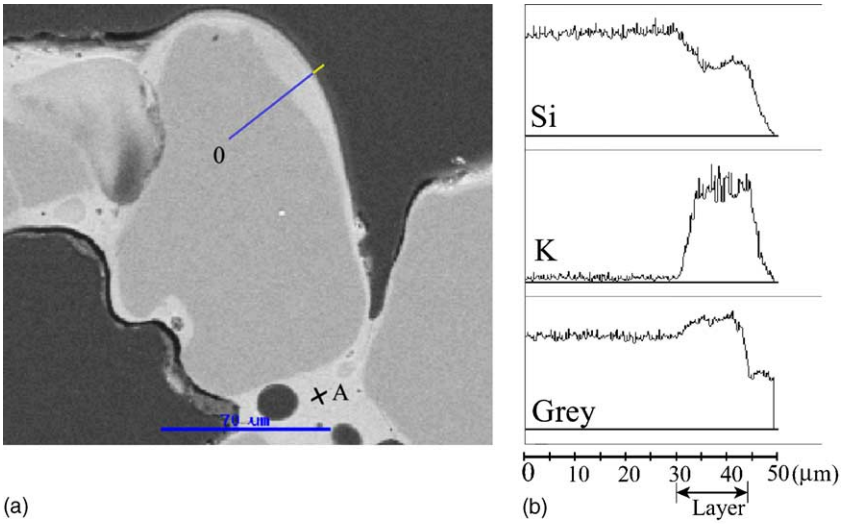

	SiO_2	Al_2O_3	Fe_2O_3	CaO	MgO	Na_2O	K_2O	SO_3	P_2O_5
Point A	62.05	0.22	0.43	7.19	0.88	0.96	22.78	0.55	3.43

Fig. 9. SEM image of cross-section of particles sampled after defluidization, at a temperature of 750 °C with an EDX analysis on the neck (point A) (a) and Si and K profile of a line scanning of the coating layer (b).

glues the particles together, but also the potassium-rich coating on the smooth grain surfaces contribute to the stickiness. The EDX analysis on point 1 was repeated with a lower accelerating voltage of the electron beam to examine if silicon underneath the coating contributes to the results of the first analysis, because the penetration length of the electrons decreases with decreasing this voltage. The two analyses show little difference, suggesting that the analysis is accurate and that the coating layer is thicker than 1 μm. The smooth appearance of the coating surface also indicates that the layer has been molten in the hot bed. These results provide a clear evidence that the presence of potassium causes the formation of the sticky sand surfaces readily for agglomeration.

In order to obtain information of the coating thickness and the elemental profile in the layer, a few samples were polished. The samples were fixed into an epoxy resin and polished with diamond sand papers of different grain size so that the cross-section of the particles can be observed. A SEM image of a polished cross-section of particles sampled after defluidization at 750 °C is shown in Fig. 9(a). It can be clearly seen that the sand grains (darker colour) were surrounded by a coating layer (lighter colour). Particles were sticked together bonded by the coatings. The coating layer is about 10–20 μm in thickness and is formed uniformly on the smooth part of the particle contour. At the concave part of particles the layer is thicker. Unlike the porous coating of coal ash on a sand grain [41], the straw ash coating shows a solid structure, indicating that the coating had been molten. EDX analysis at point A shows that the coating is potassium-rich. The composition of the coating is close to that of ash flake shown in Fig. 8, suggesting that the coatings originate from straw ash. A line scanning from the centre to the edge of the particle was performed in order to see the potassium profile inside the coating layer. The Si and K distribution along the line is plotted in Fig. 9(b). The results show that the potassium is uniformly distributed in the coating layer and that there is a steep profile at the interface between the layer and the grain. In order to obtain a quantitative elemental profile in the coating layer, EDX analyses were performed at several points along a line through the coating layer of a sand grain, which was sampled at 820 °C. The results are presented in Fig. 10 showing the similar composition to point A in Fig. 9(a). The uniformly distributed elemental profile in the layer indicates that the coating layer may be present as liquid phase during combustion, which is the main reason for agglomeration.

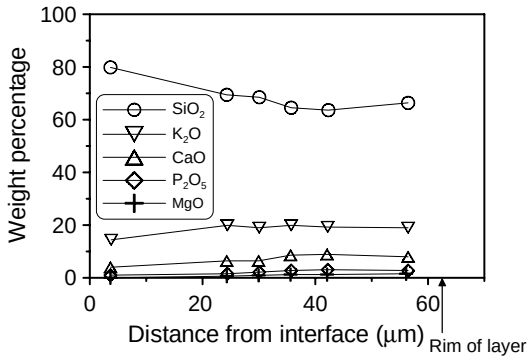

Fig. 10. Compositional profile inside the coating layer of a particles sampled after defluidization ($T = 820$ °C).

4. Discussion

During the particle sampling, it was noticed that agglomerates were formed already a few minutes after the straw feeding started. The agglomerates formed in this stage are very fragile and reveal a black ash core. The shape of these agglomerates is similar to that of straw pellets. This indicates that these agglomerates are formed around burning straw char particles. In order to verify this, batch experiments were carried out. A few straw pellets (∼0.5 g) were filled in a perforated container with 160 holes of 2 mm in diameter, which allows the sand to get in and out freely and keeps the straw pellets remaining inside. The container was inserted into the hot bed at different temperatures for various time periods and then taken out and put in a container with liquid N_2 for a quick quench. During the batch experiments, CH_4 was fired in the bed and the O_2 level was kept at 18% before the fuel pellets were introduced. The experimental conditions and visual appearance of the char/ash residues are summarized in Table 5. At low bed temperature (∼720 °C), large agglomerates were formed only 2 min after the container was inserted. The agglomerates have black cores with many sand grains on the outer surface, meaning that sand particles were caught on the burning char surface upon collision. At high temperature (∼920 °C), the formed agglomerates were stronger and with much less char after 2 min. After 10 min at 920 °C, the black cores disappeared and the agglomerates became hollow. This sample was analysed by SEM/EDX as shown in Fig. 11. The appearance of the ash and agglomerates suggests that the ash had been molten; the holes on the ash and molten surfaces provide evidence that evaporation from inside had occurred. Sand grains were either adhered to the ash or necked together by the molten layer on their surfaces. The composition on the ash surface is very similar to that of ashing at 880 °C (shown in Table 2).

During combustion, the temperature in the burning char particles can be significantly higher than that in the bed. The higher temperature causes the inorganic matters in the char particles to melt and flow out to the surfaces. When sand particles collide with a burning char particle they may adhere to it, forming an agglomerate. At lower bed temperature (∼750 °C), the burning char may be partially molten, making it adhesive and capturing sand grains upon collision. At higher temperatures (>900 °C), the burning char particles may be molten completely and behave like viscous liquid droplets. When sand grains collide with the burning particles, the liquid phase can coat on the grain surface. This may be an important way of coating formation. Another possible

Table 5
Conditions for batch experiments and visual observations of the samples

Temperature (°C)	Time (min)	Appearance of the residues in the container
724	0.5	Partially devolatilized char particles with a few sand grain on the surfaces
721	2	Char core with many sand grains on the surfaces
834	4	Hollow agglomerates consisting of sand grains, many black spots inside (unburned char)
909	2	Hollow agglomerates consisting of sand grains, many black spots inside (unburned char)
914	4	Hollow agglomerates consisting of sand grains, some small black spots inside (unburned char)
918	7	Hollow agglomerates consisting of sand grains, a few small black spots inside (unburned char)
921	10	Agglomerates of very porous structure with sand grains sintered together

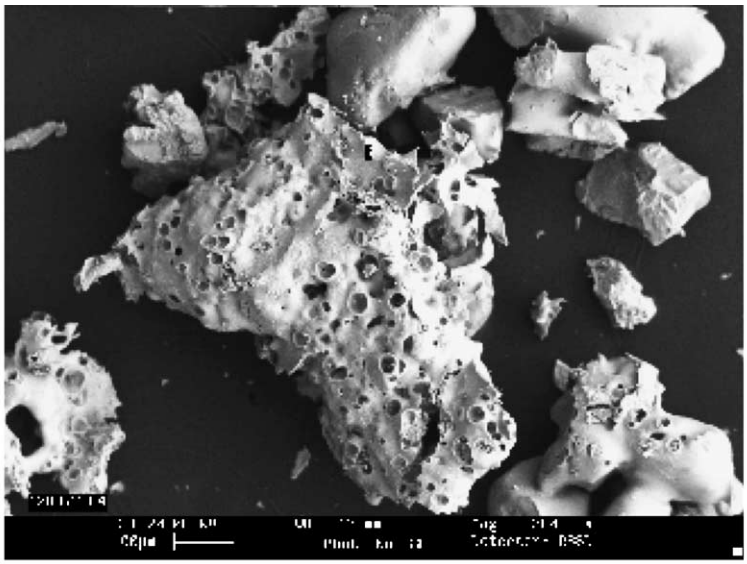

	SiO_2	Al_2O_3	Fe_2O_3	CaO	MgO	Na_2O	K_2O	SO_3	P_2O_5
Point 3 (wt.%)	51.44	0.00	1.72	10.32	2.58	1.37	27.49	1.66	3.74

Fig. 11. SEM image and an EDX analysis on the surface (point 3) of agglomerates initiated from burning char from a batch experiment.

way of the coating formation is condensation of gas phase evaporated at high temperature of burning particles to the cooler grain surfaces. The existence of the K-rich crystals on the sand surfaces reported in our early work [40], provides an evidence of this formation route.

5. Thermodynamic behaviours of straw ash under FBC conditions

Thermodynamic calculations using global equilibrium analysis were performed in order to determine the thermodynamically stable species of silicium, calcium, chlorine and sulphur, and especially potassium in straw-fired FBC with respect to agglomeration phenomena.

5.1. Thermodynamic approach

A global equilibrium analysis can be used for evaluation of ash chemistry in combustion and gasification systems. The thermodynamic calculations are made by minimizing the total Gibb's free energy of the system with a mass balance constraint. A computer program MINGTSYS of a global equilibrium analysis has been developed and applied to analyse trace elements from coal combustion [42] and deposit of potassium compounds in straw-fired utility boilers [43–45]. From this approach, the thermodynamically stable species of the elements included are determined as a function of global parameters such as, temperature, pressure and total composition. In this work, the calculations were performed to analyse the potassium distribution in a straw-fired fluidized bed combustor and the implication to agglomeration phenomena.

All calculations were performed assuming atmospheric pressure and in a temperature range 600–1100 °C. The ultimate analysis of the straw pellets listed in Table 1 and the ash analysis in Table 2 were used for the system elemental composition. A stoichiometric air to fuel factor of 1.2 was used in the calculations. In order to examine the effect of the bed material, different sand-to-straw weight ratios in a range from 0 to 100 were used in the calculations. The basic elements are C, H, O, N and S. The major inorganic species

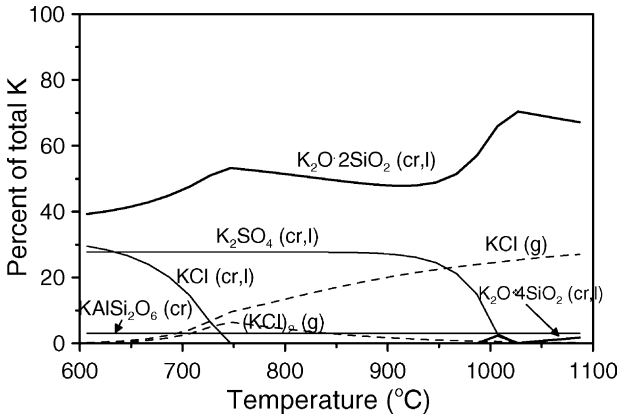

Fig. 12. Thermodynamically stable species of potassium in FBC of straw.

elements are K, Si, Cl and Ca. In some calculations, Na, Mg and P are included to study their influence on the stable K-species.

5.2. Results and discussion

The calculations are focussed on stable species of potassium, silicium, chlorine and sulphur. The results show that the sand to straw ratio has no effect on the species distribution of the main elements. The inclusion of Na, Mg and Na in the calculation has very little influence on the potassium distribution. Fig. 12 shows the thermodynamically stable potassium species as a function of temperature. The *Y*-axis gives the molar percentage of the total potassium content in the system. The symbols 'g', 'cr' and 'cr,l' denote gaseous, solid and condensed species, respectively. It is shown that at low temperature (<750 °C) the main condensed stable species of potassium are potassium chlorine (KCl), potassium sulphate (K_2SO_4) and potassium silicate ($K_2O{\cdot}2SiO_2$). The stable condensed phase of potassium sulphate keeps a constant level up to a temperature of 930 °C. In the temperature range studied, potassium silicate is the major stale potassium species, which is in the level between 40 and 70%. The potassium silicate may be molten or partly molten during combustion, forming the potassium silicate layer on the sand surface as shown from experimental results. The main stable gaseous phase potassium species are potassium chlorine either in form of monomer or dimer. The molar percentage of stable gaseous phase potassium species increases with increasing temperature and the level is below 30% in the temperature range up to 1100 °C. The calculation results are not completely in agreement with experimental results. During combustion, the gaseous KCl may condense on the surfaces of sand or ash particles in the exit zone of the reactor, where the temperature is low (<450 °C). Most of the particles in that zone will fall back to the dense bed.

It should be emphasized that the thermodynamic calculations provide only the information of the thermodynamically stable species. In the real system, the equilibrium may not be reached. In addition, the calculations are based on assumptions of pure condensed phases and an ideal gas, which can also produce some discrepancies compared to the real systems. But, the calculations did show that the major condensed phase of potassium is potassium silicates, which may provide a good guideline for assumptions of the modelling work.

6. Modelling the agglomeration phenomena in FBC

To our knowledge, no mathematical model is published to describe the agglomeration phenomena in FBC of biomass. In this work, a simple model is developed in order to describe the main characteristics of the defluidization phenomena in a straw-fired fluidized bed combustor.

6.1. Assumptions

In the fluidized bed system, particles keep moving, colliding, coalescing and breaking. After coalescence, agglomerates may also experience the strengthening or breakage. Based on these considerations and the previously described experimental results and thermodynamic calculations, the following assumptions are made:

- The agglomeration tendency is caused by the formation of a coating layer composed of potassium silicates.
- Particles of bed material are spheres with uniform size.
- The coating is equally distributed on each sphere.
- The ash content in the bed increases linearly with time.
- Agglomerates are formed by necks, whose strength develops, according to the visco-plastic sintering mechanism.
- Defluidization is a result of competition between the adhesive force and the breaking force on agglomerates.
- The breaking force on agglomerates is induced by bubbles and is proportional to the excess fluidization velocity.
- If the adhesive force is equal to or higher than the breaking force, the bed will defluidize.

6.2. Model formulation

The adhesive force between two particles caused by bonding, as illustrated in Fig. 13, can be described by:

$$F_{ad} = \pi b^2 \sigma \quad (1)$$

where π is the bonding stress and b the neck radius.

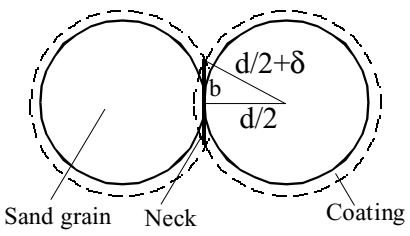

Fig. 13. Illustration of the sticky force development by sintering of the two particles.

The ash accumulation in the bed contributes to the build-up of the neck. According to the assumptions and mass balance, the thickness of the coating layer on the sand surfaces as a function of time can be expressed as:

$$n\rho_{\text{coat}}\pi d^2\delta = C_1\phi_{\text{fuel}}f_{\text{K}}t \tag{2}$$

where n is the number of sand grain, d the size of sand, C_1 the proportional constant, ϕ_{fuel} the fuel feed rate, f_{K} the weight fraction of potassium in the fuel and ρ_{coat} the density of coating. From simple geometry as shown in Fig. 13, the relation between the neck radium and coating layer thickness and the neck growing as a function of time can be obtained as:

$$b^2 = d\delta = \frac{C_1\phi_{\text{fuel}}f_{\text{K}}d^2\rho_{\text{p}}t}{6W\rho_{\text{coat}}} \tag{3}$$

where W is the sand inventory in the bed and ρ_{p} the density of the sand grains.

Since the neck will be strengthened by the visco-plastic sintering mechanism, the strength development is proportional to time and inversely proportional to the viscosity of the coating. Thus, the tensile stress of agglomerate can be written as [46]:

$$\sigma = \frac{C_2 t}{\mu d} \tag{4}$$

where μ is the viscosity of coatings. By combining Eqs. (1)–(4), the adhesion force can be expressed as:

$$F_{\text{ad}} = \frac{C_3 d t^2}{\mu} \tag{5}$$

where

$$C_3 = C_1C_2\frac{\pi\phi_{\text{fuel}}f_{\text{K}}\rho_{\text{p}}}{6W\rho_{\text{coat}}} \tag{6}$$

In a K_2O–SiO_2 system, the viscosity is dependent on the composition and temperature and can be estimated by an Arrhenius' expression [36]:

$$\mu = \mu_0 \exp\left(\frac{E_\mu}{RT}\right) \tag{7}$$

where E_μ is the activation energy for the viscosity and T the temperature.

The breaking force is assumed to be induced by bubbles and is proportional to the excess air, that is,

$$F_{\text{br}} = C_4(U - U_{\text{mf}}) \tag{8}$$

When the adhesive force, F_{ad}, is equal to the separating force, F_{br}, the bed defluidizes. Applying this to Eqs. (5), (7) and (8), we obtain the defluidization time as:

$$t_{\text{def}} = C\left(\frac{U - U_{\text{mf}}}{d}\right)^{1/2}\exp\left(\frac{E_\mu}{2RT}\right) \tag{9}$$

where

$$C = \sqrt{\frac{\mu_0 C_4}{C_3}} \tag{10}$$

Table 6
Parameters obtained for Eq. (9)

	Obtained by fitting a set of experimental data	Silicate glass (K_2O = 25 wt.%)
C [(s)$^{1.5}$]	1.11×10^{-4}	–
E_μ/R [K]	29000	22685

6.3. Results and discussion

6.3.1. Model parameters

Two parameters need to be determined in Eq. (9), the constant C and the activation energy E_μ. These two parameters were obtained by fitting to one set of experimental data with constant particle size and gas flow rate. The results are listed in Table 6. For a comparison, the activation energy for viscosity of silicate glass with 25 wt.% of K_2O obtained from the data of Bockris et al. [47] is also listed in the table. The two values are not the same but are close. The difference between the two values may be caused by the presence of a small amount of other elements in the coatings. The fitting results suggest that the model describes the ash behaviour properly. The value of C and E_μ obtained this way were used in all calculations.

6.3.2. Influence of temperature, particle size and gas velocity

From Eq. (9), the influence of temperature, fluidization velocity and particle size can be calculated. The calculated results from the model are shown in Figs. 14 and 15.

Fig. 14 plots the defluidization time as a function of temperature with different particle sizes. As the temperature increases, the sintering effect becomes dominant, resulting in a quick defluidization. The defluidization time decreases with increasing particle size partly due to the smaller surface area and thicker coating layer, and partly owing to the increase in minimum fluidization velocity. As the fluidization velocity

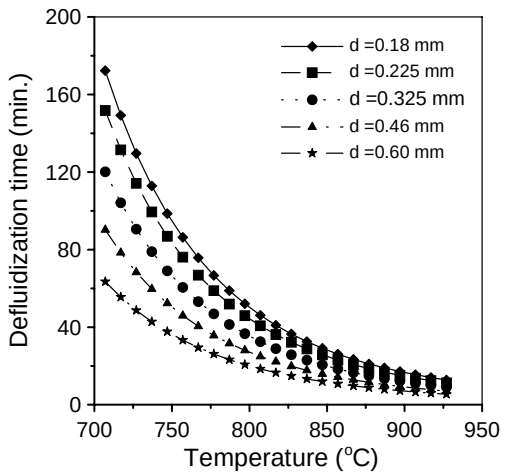

Fig. 14. Calculated defluidization time as a function of temperature with different particle size (gas flow rate = 14 N l/min).

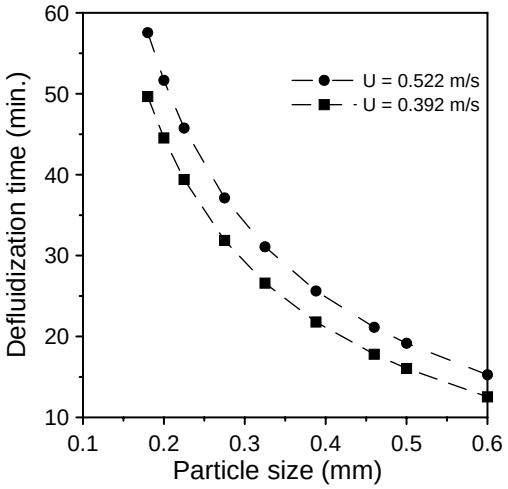

Fig. 15. Calculated defluidization time as a function of particle size with different fluidization velocity ($T = 827\,^{\circ}C$).

increases, the defluidization time can be extended as shown in Fig. 15. The trend of the influence of parameters on the defluidization time by the model is the same as the experimental findings as shown in Figs. 3 and 4.

6.3.3. Comparison with experimental data

The lines in Fig. 6 are the simulated results, which show that the lines not only follow the trend well but also give quantitative predictions at both fluidization flow rates by using the parameters in Table 6. Fig. 16 plots the calculated defluidization time versus the experimental results. The results are in a good agreement.

The model can only describe the defluidization time as a function certain important parameters. Other characteristics such as agglomeration rate or size distribution of the agglomerates cannot be simulated. More work is needed for a comprehensive model for agglomeration in FBC of biomass. Moreover, the present model describes the agglomeration process in the laboratory-scale FBC without continuous discharge of the bed material. A model for a fluidized bed combustor with a continuously operating mode is to be developed in the further work.

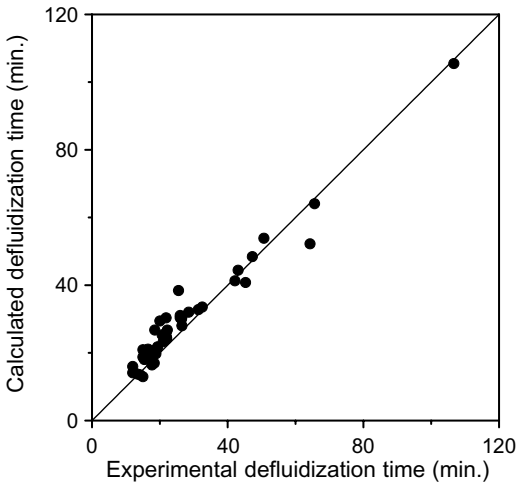

Fig. 16. Comparison of calculated defluidization time with the experimental one.

6.3.4. Initial sintering temperature

Many investigations showed the importance of the initial sintering temperature, T_s, because it is an indicator of the onset of agglomeration and is normally lower than the fusion temperature. Compo et al. [14] reported that the T_s for amorphous materials are about 80–90% of the corresponding melting temperature. However, the physical meaning of T_s is not clear. In our model, T_s was not used. A question may arise: What will happen as the temperature is close to or lower than the initial sintering temperature?

The coating layers, as shown by experiments, consist of SiO_2, K_2O and sometimes a small amount of CaO, which are typical composition of silicate glass. Fig. 17 redraws the viscosity as a function of temperature for the Si_2O–K_2O system with various weight fractions of K_2O from data of Bockris et al. [47] at high temperature range and data of El-Badry et al. [48] at low temperature range. The data follow the Arrhenius expression for both high and low temperature ranges. However, the activation energy for low temperature range is higher than that for high temperature range. It is noticed that temperatures at the cross points of the lines between the high and low temperature regions are around 700 °C. These temperatures may be considered as the initial sintering temperature for the glass or for the straw ash with the same K_2O-fraction. When temperature is decreased to the level lower than T_s, the viscosity of ash increases rapidly and the sintering effect may be negligible. In the model,

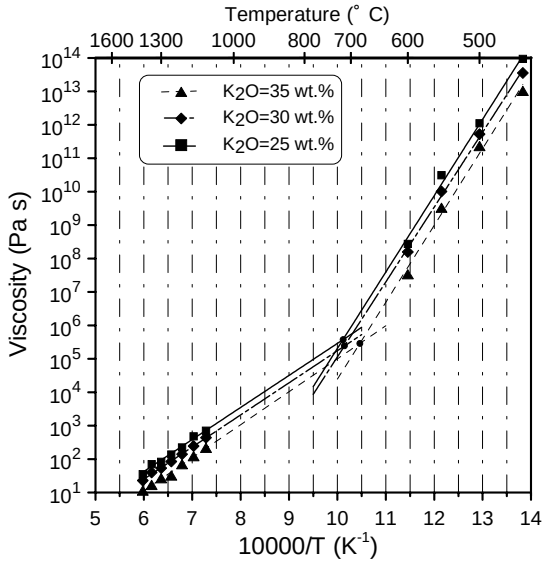

Fig. 17. Viscosity as a function of temperature in high and low temperature ranges (from [47] for high temperature range and [48] for low temperature range).

another activation energy should be used for a temperature lower than T_s. Further research is necessary to verify this.

7. Conclusions

The agglomeration and defluidization phenomena in FBC of biomass, in particular straw, are caused by the high content of potassium in the straw ash.

During combustion, the potassium in straw experiences transformation from organic and inorganic forms to various salts and amorphous of K_2O–SiO_2. Most of the potassium compounds tend to remain in the bed at temperatures below 900 °C, which are typical FBC temperatures. The melting of K_2O–SiO_2 compounds is clearly identified as the coating layer on the sand surfaces, which causes the formation of agglomerates and eventually defluidization.

The agglomeration and defluidization processes are very sensitive to temperature. A decrease in temperature can extend the defluidization time significantly, probably due to the much slower sintering of the agglomerates at lower temperatures.

It is most likely that agglomerates are initiated from burning char particles. This may be the dominant way for the potassium constituents in the ash to be transferred to the sand surfaces, forming a coating layer.

The thermodynamic equilibrium calculations show that the main stable condensed phase potassium species are potassium silicates, which agrees with the analysis of the agglomerate samples.

A simple model has been developed to describe the defluidization time as a function of parameters such as temperature, fluidization velocity and particle size. The agreement between model and experimental data is very good. More work is needed for comprehensive modelling of the agglomeration phenomena.

Acknowledgements

This work was carried out as a part of the CHEC (Combustion and Harmful Emission Control) Research Program, which is financially supported by Elsam A/S, Energi E2 A/S, the Danish and Nordic Energy Research Programmes, the European Union and the Danish Technical Research Council. The financial support of the European Commission (JOULE III, Contract JOF3-CT95-0024) to this specific project is gratefully acknowledged. Some of the SEM/EDX analyses were carried out at Danish Technological Institute (DTI). Some experiments were performed by S. Borch and M. Frankenhaeuser.

References

[1] L. Gustavsson, B. Börjesson, B. Johansson, P. Svenningsson, Reducing CO_2 emission by substituting biomass for fossil fuels, Energy 20 (1995) 1097–1113.

[2] R.D. La Nauze, A review of the fluidised bed combustion of biomass, J. Inst. Energy LX (1987) 66–76.

[3] J.L. Easterly, M. Burnham, Overview of biomass and waste fuel resources for power production, Biomass Bioenergy 10 (1996) 79–92.

[4] A.A. Wiltsee Jr., C.R. McGowin, E.E. Hughes, Biomass combustion technologies for power generation, in: Proceedings of the First Biomass Conference of the Americas, 1993, pp. 347–367.

[5] B.M. Jenkins, L.L. Baxter, T.R. Miles, T.R. Miles Jr., L.L. Oden, R.W. Bryers, E. Winther, Composition of ash deposits in biomass fueled boilers: Results of full-scale experiments and laboratory simulations, in: Proceedings of the International ASAE Summer Meeting, Kansas City, Kansas, June 19–24, 1994.

[6] E.J. Anthony, A.P. Iribarne, J.V. Iribarne, A new mechanism for FBC agglomeration and fouling when firing 100% petroleum coke, in: Proceedings of the 13th International Conference on FBC, vol. 1, 1995, pp. 523–533.

[7] J. Werther, M. Saenger, E.-U. Hartge, T. Ogada, Z. Siagi, Combustion of agricultural residues, Prog. Energy Combust. Sci. 26 (2000) 1–27.

[8] M.J. Gluckman, J. Yerushalmi, A.M. Squires, Defluidization characteristics of sticky materials on agglomerating bed, in: D.L. Keairns (Ed.), Fluidization Technol. 2 (1976) 395–422.

[9] J.P.K. Seville, R. Clift, The effect of thin liquid layers on fluidisation characteristics, Powder Technol. 37 (1984) 117–129.

[10] D. Geldart, Types of gas fluidization, Powder Technol. 7 (1973) 285–292.

[11] S. Ergun, Fluid flow through packed columns, Chem. Eng. Prog. 48 (1952) 89–94.

[12] P. Basu, A study of agglomeration of coal-ash in fluidized beds, Can. J. Chem. Eng. 60 (1982) 791–795.

[13] J.H. Siegell, High-temperature defluidization, Powder Technol. 38 (1984) 13–22.

[14] P. Compo, R. Pfeffer, G.I. Tardos, Minimum sintering temperatures and defluidization characteristics of fluidizable particles, Powder Technol. 51 (1987) 85–101.

[15] B.-J. Skrifvars, M. Hupa, M. Hiltunen, Sintering of ash during fluidized bed combustion, Ind. Eng. Chem. Res. 31 (1992) 1026–1030.

[16] B.-J. Skrifvars, M. Hupa, T. Patricainen, R. Laitinen, The effect of reducing conditions on coal ash sintering, in: Proceedings of the Engineering Foundation Conference: The impact of ash deposition on coal-fired plants, 1993.

[17] B.-J. Skrifvars, M. Hupa, R. Backman, M. Hiltunen, Sintering mechanisms of FBC ashes, Fuel 73 (1994) 171–176.

[18] B.-J. Skrifvars, M. Hupa, A. Moilanen, R. Lundqvist, Characterization of biomass ashes, in: Engineering Foundation Conference on the Application of Advanced Technology to Ash Related Problems in Boilers, Wterville Valley, NH, USA, 1995.

[19] B.-J. Skrifvars, M. Öhman, A. Nordin, M. Hupa, Predicting bed agglomeration tendencies for biomass fuels fired in FBC boilers: a comparison of three different prediction methods, Energy Fuels 13 (1999) 359–363.

[20] M.R. Dawson, C.R. Brown, Bed material cohesion and loss of fluidization during fluidized bed combustion of midwestern coal, Fuel 71 (1992) 585–592.

[21] A.R. Manzoori, E.R. Lindner, P.K. Agarwal, Inorganic transformation during the circulating fluid bed combustion of low-rank coals with high content of sodium and sulphur, in: Proceedings of the Engineers Foundation Conference on Inorganic Transformations and Ash Deposition During Combustion, 1991, pp. 735–762.

[22] A.R. Manzoori, P.K. Agarwal, The fate of organically bound inorganic elements and sodium chloride during fluidized bed combustion of high sodium, high sulphur low rank coals, Fuel 71 (1992) 513–522.

[23] E.J. Anthony, L. Jia, F. Preto, A.P. Iribarne, J.V. Iribarne, Agglomeration and fouling in petroleum coke fired boilers, in: Proceedings of the 32nd IEA FBC Conversion Meeting, Gothenborg, Sweden, 1996.
[24] M.D. Mann, K.C. Galbreath, D.P. Kalmanovitch, The role of ash chemistry and operating parameters on ash agglomeration and deposition in FBC systems, in: Proceedings of the Engineering Foundation Conference on Inorganic Transformations and Ash Deposition During Combustion, 1991, pp. 773–789.
[25] B. Olanders, B.-M. Steenari, Characterization pf ashes from wood and straw, Biomass Bioenergy 8 (1995) 105–115.
[26] A. Ergüdenler, A.E. Ghaly, Agglomeration of silica sand in a fluidized bed gasifier operating on wheat straw, Biomass Bioenergy 4 (1993) 135–147.
[27] D. Salour, B. Jenkins, M. Vafaei, M. Kayhanian, Control of in-bed agglomeration by fuel blending in a pilot scale straw and wood fuelled AFBC, Biomass Bioenergy 4 (1993) 117–133.
[28] B.D. Grubor, S.N. Oka, M.S. Ili, D.V. Daki, B.T. Arsi, Biomass FBC combustion—Bed agglomeration problems, in: K.J. Heinschel (Ed.), Proceedings of the 13th International Conference on FBC, vol. 1, 1995, pp. 515–522.
[29] A. Nordin, M. Öhman, B.-J. Skrifvars, M. Hupa, Agglomeration and defluidization in FBC of biomass fuels—Mechanisms and measures for prevention, in: Proceedings of the Engineering Foundation Conference on the Application of Advanced Technology to Ash Related Problems in Boilers, Waterville Valley, NH, USA, 1995.
[30] G. Olofsson, Z. Ye, I. Bjerle, A. Andersson, Bed agglomeration problems in fluidized-bed biomass combustion, Ind. Eng. Chem. Res. 41 (2002) 2888–2894.
[31] B. Liss, A. Blake, A.M. Squires, R. Bryson, Incipient defluidization of sinterable solids, in: D. Kunii, et al. (Eds.), Fluidization IV, 1984, pp. 249–256.
[32] G. Tardos, D. Mazzone, R. Pfeffer, Destabilization of fluidized beds due to agglomeration. I. Theoretical model, Can. J. Chem. Eng. 63 (1985) 377–383.
[33] G. Tardos, D. Mazzone, R. Pfeffer, Destabilization of fluidized beds due to agglomeration. II. Experimental verification, Can. J. Chem. Eng. 63 (1985) 384–389.
[34] J.L. Moseley, T.J. O'Brien, A model for agglomeration in a fluidized bed, Chem. Eng. Sci. 48 (1993) 3043–3050.
[35] B.J. Ennis, G. Tardos, R. Pfeffer, A microlevel-based characterization of granulation phenomena, Powder Technol. 65 (1991) 257–272.
[36] J.P.K. Seville, H. Silomon-Pflug, P.C. Knight, Modelling of sintering in high temperature gas fluidisation, Powder Technol. 97 (1998) 160–169.
[37] Y. Yang, H. Arastoopour, M.H. Hariri, A. Rehmat, Agglomeration of polyolefin particles in a fluidized bed with a central jet. II. Theory, Powder Technol. 74 (1993) 239–247.
[38] L.A. Hansen, F.J. Frandsen, K. Dam-Johansen, H.S. Sørensen, Quantification of fusion in ashes from solid fuel combustion, Thermochim. Acta 326 (1999) 105–117.
[39] H. Atakül, E. Ekinci, Agglomeration of Turkish lignites in fluidised-bed combustion, J. Inst. Energy LXII (1989) 56–61.
[40] W. Lin, G. Krushholm, K. Dam-Johansen, E. Musahl, L. Bank, Agglomeration phenomena in fluidized bed combustion of straw, in: F.D.S. Preto (Ed.), Proceedings of the 14th International Conference on FBC, 1997, pp. 831–837.
[41] A.R. Manzoori, P.A. Agarwal, The role of inorganic matter in coal in the formation of agglomerates in circulating fluid bed combustors, Fuel 72 (1993) 1069–1075.
[42] F.J. Frandsen, K. Dam-Johansen, P. Rasmussen, Tracer elements from combustion and gasification of coal—an equilibrium approach, Prog. Energy Combust. Sci. 20 (1994) 115.
[43] H.P. Michelsen, F.J. Frandsen, K. Dam-Johansen, O.H. Larsen, Deposition and high temperature corrosion in a 10 MW straw fired boiler, Fuel Process. Technol. 54 (1998) 95–108.
[44] H.P. Nielsen, L.L. Baxter, G. Sclippab, C. Morey, F.J. Frandsen, K. Dam-Johansen, Deposition of potassium salts on heat transfer surfaces in straw-fired boiler: a pilot-scale study, Fuel 79 (2000) 131–139.
[45] F.J. Frandsen, H.P. Nielsen, L.A. Hansen, P.F.B. Hansen, K.H. Andersen, H.S. Soeresen, Ash chemistry aspects of straw and coal-straw co-firing in utility boilers, in: Proceedings of the 15th Annual International Pittsburgh Coal Conference, Pittsburgh, PA, USA, 1998.
[46] S.A. Benson, M.L. Jones, J.N. Harb, Ash formation and deposition, in: L.O. Smoot (Ed.), Fundamentals of Coal Combustion—For Clean and Efficient Use, Elsevier, Amsterdam, 1993.
[47] J.O.M. Bockris, J.D. Mackenzie, J.A. Kitchener, Viscous flow in silica and binary liquid silicates, Trans. Faraday Soc. 51 (1955) 1734–1748.
[48] Kh. El-Badry, N.A. Ghoneim, H.A. El-Batal, M.M. Ammar, S. Gharib, Low-temperature viscosity of some commercial silicate glasses, Sprechsaal 114 (1981) 599–603.